RAA 2016 Vol. **16** No. **7**, 107 (14pp) doi: 10.1088/1674–4527/16/7/107
http://www.raa-journal.org *http://iopscience.iop.org/raa*

***R**esearch in*
***A**stronomy and*
***A**strophysics*

Nearby M subdwarfs from LAMOST data release 2

Yu Bai[1,2], A-Li Luo[1], Georges Comte[3], Jing-Kun Zhao[1], Hai-Feng Yang[1,4], Yan-Xin Guo[1], You-Fen Wang[1], Yin-Bi Li[1], Bing Du[1], Wen Hou[1,2], Xiao Kong[1], Zhen-Ping Yi[5], Yi-Han Song[1], Zhong-Rui Bai[1], Jian-Nan Zhang[1], Meng-Xin Wang[1], Jian-Jun Chen[1], Xiao-Yan Chen[1], Ke-Fei Wu[1], Fang Zuo[1], Yue Wu[1], Zi-Huang Cao[1], Yong-Hui Hou[6], Yue-Fei Wang[6], Yong Zhang[6]

[1] Key Laboratory of Optical Astronomy, National Astronomical Observatories, Chinese Academy of Sciences, Beijing 100012, China; *lal@nao.cas.cn*
[2] University of Chinese Academy of Sciences, Beijing 100049, China
[3] Aix-Marseille University, CNRS, Institut Pytheas, L.A.M., UMR 7326, 13388, Marseille Cedex, France
[4] School of Computer Science and Technology, Taiyuan University of Science and Technology, Taiyuan 030024, China
[5] School of Mechanical, Electrical & Information Engineering, Shandong University at Weihai, Weihai 264209, China
[6] Nanjing Institute of Astronomical Optics & Technology, National Astronomical Observatories, Chinese Academy of Sciences, Nanjing 210042, China

Received 2015 November 13; accepted 2016 January 20

Abstract We identify 108 M subdwarfs (sdMs) out of more than two hundred thousand M type spectra from the second data release (DR2) of the LAMOST regular survey. This sample, among which 58 members are identified for the first time, includes 33 extreme subdwarfs (esdMs) and 11 ultra subdwarfs (usdMs). The selection is based on the usual ratio of absorption depth of CaH2, CaH3 and TiO5 band systems. We also emphasize the use of the CaH1 band. We provide estimates of spectral subtype (SPT), Lépine metallicity index ζ, effective temperature and [Fe/H]. Both ζ–[Fe/H] and SPT–$T_{\rm eff}$ figures show reasonable consistency; compared to PHOENIX model spectra, average rounded values of [Fe/H] for sdMs, esdMs and usdMs are respectively –0.5, –1 and –1.5. The photometric distances are estimated, indicating that most sources are located within 500 pc of the Sun and 350 pc of the Galactic disk. Velocities and 3D Galactic motions are also briefly discussed. Among the 108 subdwarfs, seven stars appear to be active with a significant Hα emission line. The source LAMOST J104521.52+482823.3 is a white dwarf - M subdwarf binary, while LAMOST J123045.52+410943.8, also active, exhibits carbon features in red.

Key words: stars: late-type — stars: statistics — subdwarfs

1 INTRODUCTION

M subdwarf stars, usually denoted by 'sdM,' are stars very similar to M dwarf stars, but that exhibit lower metal abundance. Because they have a low mass and are very long-lived, they are good tracers of the primitive Milky Way and may provide important clues in understanding the Galaxy's evolution and merger history. SdMs usually range in mass from 0.075 $M_{\odot}$ to 0.3 $M_{\odot}$, and their lifetimes are greater than the Hubble time (Laughlin et al. 1997). Due to their metal deficiency, both the opacity of their outer layers and radiation pressure are very low, which makes sdMs slightly hotter (and hence bluer) and smaller than dwarfs of the same subtype (Kaler 1989). For ordinary M dwarfs, spectra of sdMs are dominated by overlapping molecular bands with complex absorption line degeneracy (Lépine et al. 2007).

A main characteristic of sdM spectra in the visible is the contrast between deep hydride bands and shallow TiO bands. Because TiO, the main contributor to atmospheric opacity in normal metallicity M stars, is a compound of two heavy elements that are depleted in subdwarfs, the spectra of the latter are rather dominated by the hydrides, especially CaH, and the ratio of hydrides to TiO increases as the metallicity of sdMs decreases. Eggen et al. (Eggen & Greenstein 1965) tried to identify sdMs with MgH and TiO bands, then Mould et al. (Mould 1976) proposed a similar method using CaH and TiO bands. A detailed definition of the most useful TiO and CaH bands was given by Reid et al. in 1995 (Reid et al. 1995, hereafter R95), providing the grounds for many subsequent sdM searches. Gizis (Gizis 1997, hereafter G97) built an M subdwarf identification and classification system using CaH1, CaH2, CaH3 and the TiO5 band. He divided the sdM sample into two groups according to their metallicity:

ordinary M subdwarfs (sdMs) and extremely metal poor M subdwarfs (esdMs). Following G97, Lépine et al. introduced an improved classification frame (Lépine et al. 2007, hereafter L07) by only using (CaH2+CaH3)/TiO5, because the CaH1 absorption band saturates for stars cooler than M3. In that work, a metallicity index ζ was defined and a new subclass, the ultra metal poor M subdwarfs (usdMs), was added. Furthermore, the index ζ proved to be overestimated and its definition and calibration were revised in 2013 (Lépine et al. 2013).

Statistical results suggest that sdMs belong to the Galactic halo and the thick disk populations (Lépine et al. 2003), and hence are expected to have large proper motions. The Lowell Proper Motion (LPM) catalog (Giclas et al. 1971), which includes 8991 stars fainter than 8 mag and with proper motions larger than $0.26''$ year^{-1}, was the first all-northern sky catalog used in early sdM sample selection. In 1976, the Luyten Half-Second (LHS) catalog was published (Luyten 1976) and then expanded in 1979 (Luyten 1979), containing 4470 stars with proper motions larger than $0.5''$ year^{-1}. Most sources in LHS are common to LPM and the catalog was revised in 2003 (Salim & Gould 2003).

In 2005, the Lépine and Shara Proper Motion (LSPM) catalog was released (Lépine & Shara 2005), in which 61 997 northern stars were included; LSPM is a considerable expansion of the LHS, with a proper motion cutoff of $0.15''$ year^{-1}. Bochanski et al. mapped the local halo with spectroscopically identified low-mass subdwarfs found in the Sloan Digital Sky Survey (SDSS), providing estimates of absolute magnitudes for sdMs. A new catalog of sdMs was published by Savcheva et al. from SDSS DR7 (2014) (Savcheva et al. 2014), which provided a large sample of 3517 new sdMs useful for statistical analysis.

However, selection biases might affect the viewpoint that sdMs mainly belong to the halo population - for example, SDSS target fields (even in the SEGUE survey) mainly cover high Galactic latitudes, favoring halo stars. We would like to make an effort to search for sdMs in more local populations such as the thin disk and discuss their properties. The Large Sky Area Multi-Object Fiber Spectroscopic Telescope (LAMOST) is now conducting the most complete spectroscopic survey of the Galactic disk (Luo et al. 2015). LAMOST DR2 contains more than 200 000 M dwarf spectra, providing great potential for discovering nearby sdMs in the Galactic disk.

In this paper, we report a search for sdMs from LAMOST DR2 and the analysis of their stellar parameters and kinematic properties. The selection of sdM candidates is presented in Section 2. Estimations of spectral subclass, metallicity index ζ, effective temperature and [Fe/H] are detailed in Section 3. Extinction, distance and total velocity of our candidates are calculated in Section 4. In Section 5, seven active sdMs with a significant Hα emission line sample are discussed, including a white dwarf - subdwarf binary. Finally, a summary is given in Section 6.

Table 1 Spectral Features (Reid et al. 1995)

Band	Feature Band	Pseudocontinuum
CaH1	6380–6390	6345–6355
CaH2	6814–6846	7042–7046
CaH3	6960–6990	7042–7046
CaOH	6230–6240	6345–6354
TiO5	7126–7135	7042–7046

2 SAMPLE SELECTION AND REDUCTION

LAMOST (Cui et al. 2012), a 4 m-class telescope, characterized by both a large field of view (5°) and large aperture (3.6 m - 4.9 m), is a powerful instrument dedicated to astronomical studies of large samples. The DR2 of the regular survey contains 226 985 M type spectra with a resolution of R $\sim$ 1800. Our sdM sample was selected from this subset, using only spectroscopic criteria.

In the visible, the most prominent features in sdM spectra are the deep hydride bands and the shallow TiO bands. A very easy way to separate sdMs from ordinary M dwarfs is to search for two bands with a 'W'-like shape within $6000 \sim 7000$ Å (Fig. 1). The first is around 6200$\sim$6400 Å, basically formed by CaOH and CaH1, and the other is around 6800$\sim$7000 Å, principally formed by CaH2 and CaH3. The red leg of the 'W' gets deeper as the metallicity gets lower. The spectral features and indices we used are listed in Table 1, and the index definition we adopted is the "Hammer" one (Covey et al. 2007):

$$\text{line index} = \frac{\text{Mean Flux of F}}{\text{Mean Flux of P}}\,, \tag{1}$$

where F is the feature band and P is the local pseudocontinuum.

Because sdMs are intrinsically very faint stars whose absolute magnitude in the r band is > 10, we did not want to exclude low signal-to-noise (S/N) spectra. Subject to the observational limitations in apparent magnitude, the difficulties of accurate sky subtraction at wavelengths longer than 8000 Å and the selection criteria of the LAMOST survey, there might not be very many sdM candidates found and those that might be found are expected to be early types (with $T_{\rm eff} > 3200$ K). We chose to combine the two search criteria given respectively by G97 and L07 to ensure a reasonable completeness. Thus, a spectrum was selected when it satisfied any one of the next two conditions:

$$\begin{aligned}\text{CaH1} \;<\; & 0.695 \times \text{TiO5}^3 - 0.818 \times \text{TiO5}^2 \\ & +0.413 \times \text{TiO5} + 0.651\,,\end{aligned} \tag{2}$$

$$\zeta = \frac{1 - \text{TiO5}}{1 - [\text{TiO5}]_{Z_\odot}} < 0.825\,, \tag{3}$$

where $[\text{TiO5}]_{Z_\odot}$ = –0.588(CaH2+CaH3)^3+2.211(CaH2+CaH3)^2 –1.906(CaH2+CaH3)+0.622 (Lépine et al. 2013).

CaH1, CaH2, CaH3 and TiO5 were automatically measured on all the spectra and the ζ value was subsequently computed. A check was performed on a subsample of 1541 previously known M dwarfs that are common to

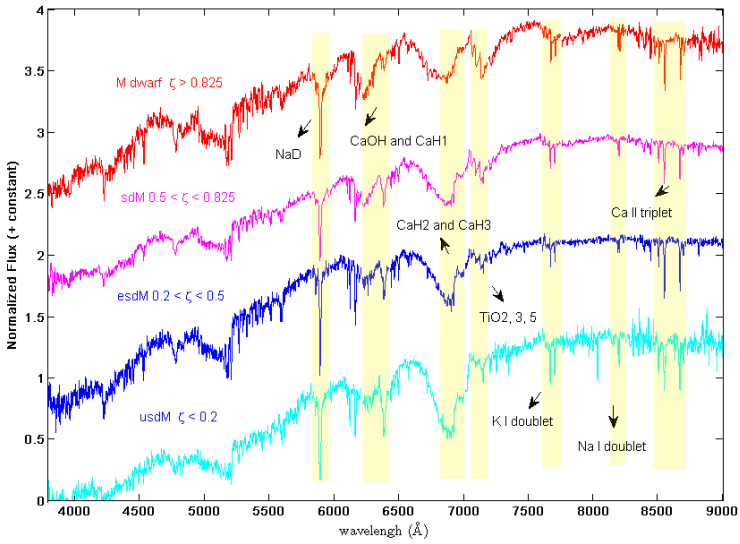

Fig. 1 Example spectra from LAMOST of an M dwarf, sdM, esdM and usdM, from top to bottom respectively. A significant feature of sdMs is that the depth ratio of the CaH bands to the TiO bands increases as the metallicity decreases.

the LAMOST and SDSS databases to evaluate the consistency of the Hammer indices of these four molecular bands from the two instruments. Figure 2 shows the results of this check, underlining an excellent consistency with rather small random differences and systematic deviations, and Gaussian distributions of the differences. The three CaH bands were used simultaneously to avoid the misclassification of spectra resulting from accidental estimation errors in the Hammer indices. Moreover, CaH1 proved very useful to help confirm an sdM candidate in the final phase of selection by visual examination. After the fully automated preliminary screening, 15 000 spectra were selected. Each one was then scrutinized by eye. Objects where CaH1 was deeper than the neighboring CaOH band were also retained as sdM candidates because the CaOH feature vanishes at low metallicity (see Fig. 1). The final list, containing only 108 candidates, was cross-matched with several catalogs: SDSS (York et al. 2000), 2MASS (Skrutskie et al. 2006) and USNO-B (Monet et al. 2003) for g, r, i, z magnitudes, J, H, K magnitudes, B, R, I magnitudes and proper motions. Radial velocities were extracted from the LAMOST catalog and an estimate of the interstellar extinction was computed from the Schlegel et al. dust maps (Schlegel et al. 1998) (see also Section 4 below). Eleven objects had been previously targeted by SDSS fibers and we could check the characteristic subdwarf features in their SDSS spectra: they are displayed in Table 2. The complete catalog is available in the online version of the journal.

3 SPECTRAL SUBTYPE AND METALLICITY SUBCLASS

Within the scheme of Lépine et al. (2007), we can assign a spectral subtype (SPT) using a combination of only CaH2 and CaH3. The following polynomial can be used to identify the SPT. We recall that with this definition, SPT $= 0$ corresponds to an M0 star, SPT < 0 is for K5–K7 stars and SPT > 0 is for stars later than M0. Derived values for the SPT are listed in Table 2.

$$\mathrm{SPT} = 1.4(\mathrm{CaH2}+\mathrm{CaH3})^2 - 10.0(\mathrm{CaH2}+\mathrm{CaH3}) + 12.4. \quad (4)$$

Also, the metallicity subclass of an sdM is defined by its index ζ which may be used to divide the subdwarfs into metallicity subclasses as: ordinary (metal-rich) dwarf when $\zeta > 0.825$, subdwarf when $0.5 < \zeta < 0.825$, extreme subdwarf when $0.2 < \zeta < 0.5$ and ultra subdwarf when $\zeta < 0.2$. We list the Lépine et al. metallicity index in Table 2. Among our 108 stars, there are 64 sdMs, 33 esdMs and 11 usdMs, with the latter being only early-type objects (K7 to M0).

Within a common luminosity class, a strong correlation is expected between the spectral type or subtype of an object and its effective temperature (hereafter $T_{\rm eff}$). The index ζ, describing the deficiency of TiO5 absorption with respect to the solar metallicity TiO5 reference, is expected to be tightly correlated to the usual standard metallicity [Fe/H]. But for M type stars, due to their complex spectra with many overlapping molecular bands, the accurate determination of $T_{\rm eff}$ and [Fe/H] remains a problem. We tried to match our candidates to PHOENIX model spectra (Allard & Hauschildt 1995), so as to assess estimates of $T_{\rm eff}$ and [Fe/H] for all objects in our sample.

To simplify the matching process, we simply computed the deviation between the observed spectrum of an object and models of the PHOENIX grid, then chose the nearest model as being the best fitting one. The $T_{\rm eff}$ step of the PHOENIX grid is 100 K while the [Fe/H] step is 0.5 dex, and we only used models with $\log g = 5.0$. Hence, since we do not try to produce interpolated values,

Table 2 Derived Parameters of the 108 sdMs

LAMOST ID	SPT	$T_{\rm eff}$ (K)	ζ	[Fe/H]	LAMOST ID	SPT	$T_{\rm eff}$ (K)	ζ	[Fe/H]
(1)	(2)	(3)	(4)	(5)	(6)	(7)	(8)	(9)	(10)
J000530.87+031735.8	0	3700	0.912	−0.5	J083012.38+332105.1 (*)	0.5	3600	0.156	−1
J003023.63+050904.1	−0.5	3700	0.247	−1	J084127.90−011403.2	0	3700	0.816	−0.5
J003010.59+400741.0	1	3600	0.793	−0.5	J084542.20+252123.5	−0.5	3800	0.032	−0.5
J003956.41+370159.1	0.5	3600	0.739	−0.5	J084601.17+272302.0	2	3500	0.507	−0.5
J004143.13+312729.9	0.5	3600	0.444	−1	J091406.72+305034.3	0	3700	0.589	−0.5
J004613.83+335010.3	1	3500	0.322	−1	J092725.42+171101.0	1	3600	0.631	−0.5
J005242.36+315545.1	0	3700	0.179	−1	J093756.59+283917.0	−0.5	3800	0.822	−0.5
J012100.34−012517.0	2	3500	0.655	−0.5	J093941.97+275140.9	1	3500	0.386	−1
J012534.63−041817.6	0.5	3700	0.435	−0.5	J095451.13+085152.7	−0.5	3800	0.745	−0.5
J012615.42+352030.6	0.5	3600	0.653	−0.5	J095805.56+333801.5	0	3800	0.828	−0.5
J014614.53+010035.0	0.5	3500	−0.335	−1	J101247.46+274729.5 (*)	2	3500	0.836	−0.5
J022353.40+045251.3	0.5	3500	0.278	−1	J102351.13+320401.8	0.5	3700	0.707	−0.5
J023243.54+073557.0	0	3700	0.613	−0.5	J102516.09+461745.8	2	3700	0.815	0
J023252.09+505139.4	2	3400	0.020	−1.5	J103528.96+423846.0	0.5	3600	0.383	−1
J023608.53+095440.9	2	3600	0.589	−0.5	J104049.04+290539.3 (*)	0	3700	0.592	−0.5
J024208.23+065529.0	−0.5	3800	0.444	−0.5	J104352.42+303649.3 (*)	2	3400	0.179	−1.5
J030114.52+244228.6	1	3500	0.234	−1	J104521.52+482823.3	3	3400	0.719	−0.5
J031703.00+240118.8	0	3800	0.611	−0.5	J105220.46+274313.1	−0.5	3800	0.559	−0.5
J032255.61+244336.5	0	3800	0.444	−0.5	J105240.29+283353.8	0	3700	0.236	−1
J032348.69+243229.4	−0.5	3800	0.546	−0.5	J105736.90+473807.5 (*)	0	3600	0.270	−1
J034751.81+254730.6	2.5	3400	0.750	−0.5	J105753.97+272644.0	−0.5	4000	1.157	0
J035113.75+281105.1	−0.5	3800	0.526	−0.5	J110717.83+273252.0	0	3900	0.728	−0.5
J040301.53+153227.2	0	3800	0.976	−0.5	J112129.19+073443.2	0	3600	0.416	−1
J041112.01+011826.0	0	3700	0.441	−0.5	J112811.03+535521.6	1	3500	0.402	−1
J041726.96+281947.9 (*)	0.1	3500	−0.091	−1.5	J113108.72+540535.4	0.5	3700	0.452	−0.5
J044738.31+273601.0	0.5	3600	0.733	−0.5	J115646.82+593904.9	0	3700	0.344	−0.5
J050512.20+304322.8	2.5	3400	0.479	−0.5	J115914.12+580528.5	−1	3900	0.708	−0.5
J053434.17+221250.6	−1.5	4000	0.181	−0.5	J120229.03+264514.8	−1	3900	0.545	−0.5
J055612.53+243730.8	2	3500	0.465	−0.5	J121434.23+584523.4 (*)	3	3500	0.266	−1
J055710.69+343159.8	−0.5	3800	0.795	−0.5	J121546.28+324433.1	0.5	3700	0.824	−0.5
J061642.18+364838.6	1	3600	0.622	−0.5	J121956.41+273337.9	0	3700	0.931	−0.5
J062334.67+265644.1	0.5	3700	0.742	−0.5	J123045.52+410943.8 (*)	1.5	3500	0.225	−1
J062413.45+335651.4	0	3800	1.017	−0.5	J124754.95+114026.0	−0.5	3800	0.505	−0.5
J062500.70+305648.7	0.5	3600	0.476	−0.5	J125203.78+540656.1	0.5	3700	0.484	−0.5
J063137.07+331035.6	0	3800	0.678	−0.5	J125207.81+003708.6	−0.5	3700	0.461	−1
J063216.36+263137.5 (*)	2	3500	0.411	−0.5	J125648.36+394429.1	0	4000	0.772	0
J063257.83+323450.5	0	3600	0.326	−1	J131006.33+201951.7	0	3700	0.134	−1
J063347.51+235036.2	−0.5	3800	0.558	−0.5	J131754.25+191846.2	0	3700	0.825	−0.5
J065045.65+521346.8	1	3600	0.584	−0.5	J132823.09+090226.8	1.5	3900	0.746	0
J070025.94+265335.1	1.5	3400	0.186	−1	J133222.33+185719.8	0	3700	0.857	−0.5
J071033.86+271818.2	1	3800	0.760	0	J140505.50+162647.2 (*)	3.5	3400	0.572	−0.5
J071424.09+273918.4	−0.5	3700	0.223	−1	J141935.25+504216.3	0	3800	0.663	−0.5
J071753.80+354038.8	−1	3900	0.539	−0.5	J142332.60+231801.0	0	3900	0.762	−0.5
J071758.85+354257.0	0	3800	0.471	−0.5	J142714.04+335957.7	0.5	3700	0.641	−0.5
J072320.04+253610.9	−0.5	3800	0.002	−0.5	J145636.05+312454.7	0.5	3700	0.724	−0.5
J072516.99+290323.3	−0.5	3800	0.693	−0.5	J145811.86+311508.5	0.5	3600	0.570	−0.5
J073835.27+343953.5	0.5	3700	0.617	−0.5	J151637.89+340322.6	2.5	3400	0.639	−0.5
J074444.97+272648.2	−0.5	3800	0.567	−0.5	J154919.39+001316.1	−0.5	4000	0.717	0
J074655.54+281323.6	−0.5	3900	1.011	0	J170252.10+330952.2	0	3800	0.518	−0.5
J074656.72+215025.9	−1	3900	0.479	−0.5	J172012.34+242931.7	3.5	3300	0.555	−1
J075423.94+290739.1	−1	3800	0.394	−0.5	J220747.72+001606.0 (*)	0	3700	0.482	−0.5
J075852.18+215135.0	0.5	3600	0.466	−0.5	J225612.76+061236.3	2	3500	0.528	−0.5
J075920.76+525928.1	0.5	3600	0.843	−0.5	J230312.72+044430.7	0	3700	0.666	−0.5
J080633.27+321145.4	3.0	3400	0.477	−0.5	J235409.68+281720.2	−0.5	3800	0.655	−0.5

Notes: The SPT results are rounded to 0.5, and objects already known from SDSS are marked with an asterisk in Cols. (1) and (6).

the adopted $T_{\rm eff}$ and [Fe/H] values for our stars will be rounded. In practice, subject to various perturbations such as reddening, flux calibration problems, poor S/N, etc, observed spectra usually exhibit low order distortion compared with their optimally fitted model spectra. We introduce a binomial to fit the ratio vector of an observed spectrum to the model spectrum. Fitting with the PHOENIX grid using a least squares algorithm, we thus derive the parameters of the best model corresponding to each star, which is expected to be close to the real values of the parameters of that target. The $T_{\rm eff}$ and [Fe/H] found are listed in Table 2.

To assess the errors on the derived parameters, we conduct the template matching experiment thrice, with different spectral bands (6000∼7500 Å, 6000∼8500 Å and 5500∼8000 Å) and different weights of the feature bands

Table 3 Observed Magnitudes and Adopted Extinction for the 108 sdMs

LAMOST ID	g	r	i	z	J	B	R	I	V	3D_A_r
J000530.87+031735.8	18.97	17.58	16.91	16.54	15.33	19.11	17.19	15.87	17.55	0
J003010.59+400741.0	17.24	15.72	14.97	14.52	13.34	18.02	15.28	14.1	16.53	0
J003023.63+050904.1	18.44	16.88	16.22	15.81	14.6	18.96	16.55	15.92	17.85	0
J003956.41+370159.1	16.48	14.97	14.22	13.78	12.57	17.2	14.5	13	15.3	0
J004143.13+312729.9	19.31	17.74	17.06	16.64	15.44	18.89	17.36	16.14	18.21	0
J004613.83+335010.3	17.63	16.04	15.27	14.84	13.63	18.7	-	-	16.7	0
J005242.36+315545.1	18.44	16.93	16.28	15.88	14.72	18.4	16.35	15.29	17.48	0
J012100.34–012517.0	18.99	17.41	16.53	16.02	14.83	18.97	17.09	-	17.67	0
J012534.63–041817.6	19.13	17.59	16.88	16.48	15.25	18.87	16.65	16.33	17.61	0
J012615.42+352030.6	18.72	17.19	16.44	16.03	14.86	18.9	16.69	-	17.85	0
J014614.53+010035.0	19.32	17.77	17.09	16.66	15.5	19.36	17.04	16.93	18.8	0
J022353.40+045251.3	19.34	17.77	17.03	16.59	15.36	20.16	17.59	16.66	19	0
J023243.54+073557.0	19.15	17.67	16.86	16.49	15.15	18.35	16.82	-	17.88	0
J023252.09+505139.4	14.46	13.49	13.19	12.97	11.82	15.05	13.43	12.51	13.49	0
J023608.53+095440.9	18.35	16.87	16.12	15.75	14.43	18.46	16.66	15.47	17.57	0
J024208.23+065529.0	18.81	17.22	16.5	16.09	14.85	18.62	16.54	15.25	17.08	0
J030114.52+244228.6	18.16	16.59	15.82	15.46	14.22	18.29	16.32	15.13	17.33	0.15
J031703.00+240118.8	19.19	17.61	16.9	16.54	15.17	20.18	16.99	16.39	18.73	0.29
J032255.61+244336.5	18.3	16.85	16.19	15.88	14.63	20.71	17.66	16.98	17.7	0.09
J032348.69+243229.4	19.24	17.65	17	16.65	15.07	18.59	15.98	15.01	17.4	0.19
J034751.81+254730.6	17.24	15.73	14.75	14.27	12.91	17	15.5	13.9	16.27	0.27
J035113.75+281105.1	18.46	16.98	16.3	15.96	14.61	19.37	16.56	15.77	18.11	0
J040301.53+153227.2	17.52	16	15.29	14.87	13.63	17.56	15.77	-	16.72	0.22
J041112.01+011826.0	22.7	21.39	19.92	18.94	15.24	18.57	16.86	16.73	18.48	0.04
J041726.96+281947.9	17.31	15.71	15.05	14.68	13.53	17.6	16.3	-	17.03	0
J044738.31+273601.0	16.25	14.75	14.15	13.67	12.32	16.42	14.44	13.67	15.48	0.28
J050512.20+304322.8	20.23	19	18.48	18.2	16.83	20.65	19.02	-	19.9	0.32
J053434.17+221250.6	18.88	17.36	16.72	16.38	15.09	18.4	16.63	15.89	17.65	0
J055612.53+243730.8	19.71	18.09	17.27	16.77	15.4	20.25	17.96	16.14	17.47	0.18
J055710.69+343159.8	17.41	15.94	15.3	15.01	13.76	18.33	15.78	14.4	16.74	0.12
J061642.18+364838.6	15.91	14.41	13.7	13.24	11.81	16.06	14.46	12.81	14.21	0
J062334.67+265644.1	18.96	17.5	16.76	16.33	15.16	19.37	16.67	15.83	17.27	0.11
J062413.45+335651.4	17.6	16.46	15.8	15.47	14.16	17.7	16.13	-	16.99	0
J062500.70+305648.7	18.3	16.78	16.06	15.69	14.37	18.24	16.09	15.38	17.23	0.11
J063137.07+331035.6	19.1	17.61	16.9	16.56	15.26	19.38	17.48	16.3	18.53	0.15
J063216.36+263137.5	19.95	18.33	17.48	16.99	15.7	20.2	18.42	16.92	19.54	0.05
J063257.83+323450.5	19.54	18	17.35	17.01	15.89	19.4	17.62	16.96	18.57	0.36
J063347.51+235036.2	17.11	15.66	15	14.73	13.5	17.87	15.6	14.12	15.62	0
J065045.65+521346.8	15.55	13.8	13.11	12.79	11.4	15.43	13.55	12.87	14.57	0
J070025.94+265335.1	19.44	17.9	17.11	16.72	15.45	20.29	17.36	15.98	18.35	0.12
J071033.86+271818.2	18.6	17.11	16.32	15.93	14.58	18.74	16.3	16.47	16.93	0.04
J071424.09+273918.4	16.62	15.18	14.55	14.26	13	16.93	14.96	13.8	15.87	0
J071753.80+354038.8	17.69	16.27	15.65	-	14.17	-	16.05	-	17.08	0
J071758.85+354257.0	19.26	17.75	17.03	-	15.39	18.34	17.48	16.4	17.8	0
J072320.04+253610.9	17.3	15.85	15.18	14.81	13.64	16.93	14.39	-	15.75	0.03
J072516.99+290323.3	15.87	14.41	17	13.4	12.2	-	-	-	17.91	0
J073835.27+343953.5	18.13	16.63	15.92	15.48	14.32	18.88	16.38	15.02	17.75	0
J074444.97+272648.2	19	17.51	16.81	16.39	15.14	19	17.38	15.96	17.54	0
J074655.54+281323.6	19.55	18.2	17.63	17.29	15.6	19.06	17.02	16.23	17.32	0
J074656.72+215025.9	16.9	15.51	14.92	14.59	13.42	16.81	15.77	14.19	16.34	0
J075423.94+290739.1	18.92	17.54	16.92	16.54	15.48	18.96	17.25	16.33	17.39	0.02
J075852.18+215135.0	19.03	17.52	16.75	16.32	15.18	19.62	17.27	16.42	18.79	0.03
J075920.76+525928.1	17.15	15.64	14.85	14.41	13.18	16.95	15.41	14.32	16.46	0
J080633.27+321145.4	19.2	17.51	16.51	15.93	14.72	18.6	16.9	15.6	17.74	0.04
J083012.38+332105.1	18.31	16.71	16.02	15.64	14.43	18.23	16.06	15.1	17.23	0
J084127.90–011403.2	15.26	13.82	13.17	12.77	11.5	15.51	13.43	12.31	14.19	0
J084542.20+252123.5	18.84	17.36	16.71	16.35	15.14	18.89	17.26	16.13	17.12	0
J084601.17+272302.0	19.03	17.52	15.8	14.88	14.64	18.8	16.5	15.6	17.87	0.01
J091406.72+305034.3	17.11	15.64	14.99	14.63	13.41	17.19	15.35	14.04	15.75	0
J092725.42+171101.0	19	17.46	16.71	16.28	15.08	19.18	16.92	16.05	18.14	0
J093756.59+283917.0	18.65	17.17	16.51	16.13	14.93	18.14	16.78	15.87	16.74	0
J093941.97+275140.9	18.74	17.16	16.42	15.97	14.74	18.14	16.89	15.83	17.55	0

Table 3 — *Continued.*

LAMOST ID	g	r	i	z	J	B	R	I	V	3D_A_r
J095451.13+085152.7	18.14	16.7	16.07	15.71	14.59	18.06	16.26	15.41	16.61	0
J095805.56+333801.5	19.04	17.6	16.95	16.56	15.36	19.05	17.69	16.74	18.4	0
J101247.46+274729.5	18.7	17.1	16.17	15.66	14.4	18.51	16.84	15.57	16.97	0
J102351.13+320401.8	16.96	15.44	14.71	14.3	13.1	17.91	15.17	13.71	16.66	0
J102516.09+461745.8	18.93	17.33	16.32	15.75	14.45	19.48	17.12	15.65	17.84	0
J103528.96+423846.0	16.31	14.79	14.03	13.57	12.16	16.88	14.54	13.15	14.65	0
J104049.04+290539.3	18.58	16.83	16.05	15.63	14.39	18.46	16.71	15.4	17.67	0
J104352.42+303649.3	20.01	18.32	17.56	17.11	15.94	20.18	17.8	17.03	19.21	0
J104521.52+482823.3	18.15	17.35	16.51	15.99	14.7	19.3	17.05	15.78	18.29	0
J105220.46+274313.1	19.06	17.59	16.93	16.57	15.35	18.76	17.2	16.35	18.06	0
J105240.29+283353.8	19.12	17.61	16.91	16.5	15.39	19.12	16.88	16.29	17.97	0
J105736.90+473807.5	18.51	16.91	16.21	15.81	14.63	19.54	16.61	15.4	17.86	0
J105753.97+272644.0	19.08	17.7	17.03	16.64	15.42	18.83	19.09	16.1	17.24	0
J110717.83+273252.0	17.88	16.53	15.96	15.65	14.49	18.23	16.07	15.19	16.53	0
J112129.19+073443.2	19.91	18.25	17.41	16.89	15.53	20.52	18.15	17.15	19.4	0
J112811.03+535521.6	19.04	17.48	16.72	16.31	15.16	19.07	17.13	16	18.18	0
J113108.72+540535.4	19.73	18.22	17.48	17.08	15.92	19.82	17.99	17.42	17.97	0
J115646.82+593904.9	18.39	16.94	16.26	15.9	14.69	18.81	17	15.77	17.39	0
J115914.12+580528.5	17.95	16.59	16	15.69	14.47	18.49	16.37	15.52	17.53	0
J120229.03+264514.8	16.78	15.38	14.81	14.47	13.3	16.87	15.23	14.04	15.47	0
J121434.23+584523.4	18.55	16.92	16.2	15.79	14.52	18.69	16.52	15.59	17.69	0
J121546.28+324433.1	18.91	17.45	16.75	16.34	15.2	18.66	16.87	16.31	17.87	0
J121956.41+273337.9	18.46	16.99	16.29	15.9	14.62	18.27	16.5	15.01	17.45	0
J123045.52+410943.8	18.56	16.69	15.95	15.5	14.09	18.82	16.53	15.32	17.38	0
J124754.95+114026.0	17.69	16.23	15.6	15.25	14.05	17.69	-	-	16.49	0
J125203.78+540656.1	18.35	16.77	16.01	15.6	14.34	17.04	15.99	14.48	16.54	0
J125207.81+003708.6	18.17	16.67	15.98	15.61	14.32	18.51	16.24	15.29	16.73	0
J125648.36+394429.1	15.77	14.41	14.19	13.47	12.31	15.9	14.06	12.23	14.97	0
J131006.33+201951.7	16.5	15.07	14.44	14.1	12.86	16.57	14.85	13.67	15.59	0
J131754.25+191846.2	17.47	15.93	15.19	14.77	13.54	17.43	15.69	14.09	16.62	0
J132823.09+090226.8	17.31	15.74	16.06	14.32	13.07	17.76	15.12	13.07	16.31	0
J133222.33+185719.8	16.95	15.5	14.79	14.41	13.2	18.04	15.26	13.58	16.76	0
J140505.50+162647.2	20.41	18.79	17.75	17.16	15.93	19.42	18.21	17.2	19.93	0
J141935.25+504216.3	16.72	15.23	14.55	14.16	12.96	16.85	15.02	13.68	15.77	0
J142332.60+231801.0	18.04	16.63	15.99	15.62	14.41	18.63	15.7	15.01	16.9	0
J142714.04+335957.7	18.58	17.06	16.33	15.95	14.77	18.4	16.76	-	17.65	0
J145636.05+312454.7	19.26	17.79	17.08	16.69	15.62	18.96	17.25	16.52	18.23	0
J145811.86+311508.5	18.56	16.97	16.24	15.82	14.62	17.6	-	-	17.3	0
J151637.89+340322.6	18.84	17.28	16.33	15.82	14.56	19.02	17.16	15.73	17.57	0
J154919.39+001316.1	15.24	13.94	16.71	13.03	11.85	18.35	13.37	12.48	15.28	0
J170252.10+330952.2	15.85	13.67	13.08	13.43	11.3	15.26	13.34	12.7	14.15	0
J172012.34+242931.7	18.05	16.33	15.29	14.7	13.38	18.2	16.13	-	17.24	0
J220747.72+001606.0	19.37	17.76	16.95	16.5	15.31	19.63	17.65	16.44	18.84	0
J225612.76+061236.3	18.57	16.95	16.09	15.6	14.33	19.28	17.22	14.93	16.99	0
J230312.72+044430.7	19.12	17.59	16.85	16.43	15.15	19.6	17.72	15.7	18.73	0
J235409.68+281720.2	16.59	15.08	14.45	14.12	12.88	16.02	13.63	13.31	14.9	0

Table 4 Absorption Lines for RV Estimation (Reid et al. 1995)

Line	Center	Line	Center	Line	Center
KI	7667.0089	NaI	8185.5054	CaII 8500.36	CaII 8644.52
KI	7701.0825	NaI	8197.0766	CaII 8544.44	

(the weighted values for CaH and TiO bands are 1.5, 2 and 2.5 while the values for other bands are 1.0). It turns out that the derived $T_{\rm eff}$ and [Fe/H] are exactly equal (i.e. the same model is the nearest to the real spectrum) except for two stars with a 100 K difference in $T_{\rm eff}$ and a 0.5 dex difference in [Fe/H]. Finally, in Figure 3 we compare the SPT with $T_{\rm eff}$, and ζ with [Fe/H] derived from the model spectra. The consistency between the observed spectral indicators (SPT and ζ) and model-derived spectral parameters is reasonable, while showing appreciable dispersion. In brief, the relationship between SPT and $T_{\rm eff}$ can be modeled with a third order polynomial while the approximate average values of [Fe/H] for sdMs, esdMs and usdMs are respectively -0.5, -1 and -1.5, which are quite consistent with the conclusion by Lépine et al. (2007) and Woolf et al. (2009). The coolest object found is J172012.34+242931.7,

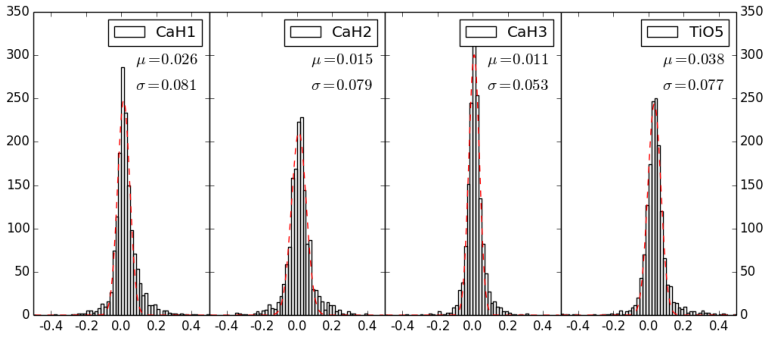

Fig. 2 Comparison of spectral indices CaH and TiO5 measured on LAMOST and SDSS spectra. The histograms represent the distribution of the differences in $\mathrm{index_{LAMOST}} - \mathrm{index_{SDSS}}$. The dotted red line is the fitted Gaussian distribution with mean μ and standard deviation σ.

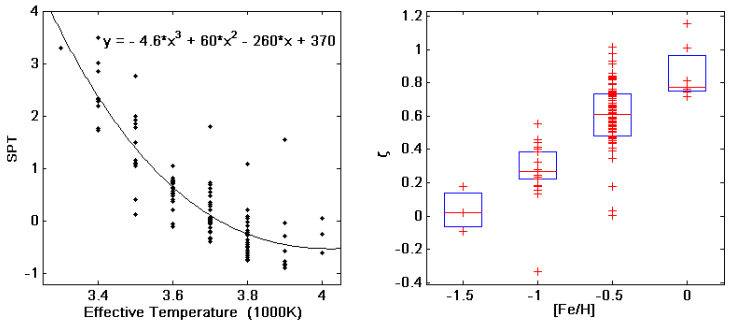

Fig. 3 *Left panel*: Relation between SPT and $T_{\rm eff}$, with a curve fitted by a third order polynomial. *Right panel*: Relation between the Lépine et al. metallicity index ζ and [Fe/H].

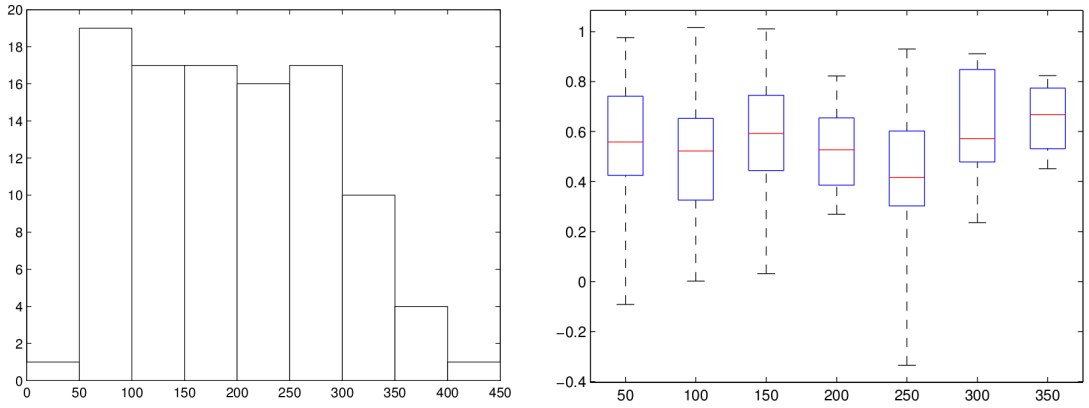

Fig. 4 *Left panel*: Histogram of distances of all sdMs in the sample, with the X-axis in pc. *Right panel*: Distribution of metallicity index ζ with the height above the Galactic plane $Z_{\rm gal}$. The unit used on the X-axis is pc.

an sdM with an SPT of 3.5 and a $T_{\rm eff}$ of 3300 K. For five objects, the closest model spectrum was a solar-metallicity one, although the selection criteria were met to classify them as subdwarfs (see Fig. 3).

4 MAGNITUDES, EXTINCTION, DISTANCE AND TOTAL VELOCITY

4.1 Magnitudes and Extinction

2MASS J, H, K magnitudes are available for all 108 sdMs in our sample, while 82 of them have accurate SDSS photometry with u, g, r, i, z. The remaining 26 stars have Pan-STARRS1 g, r, i, z magnitudes, whose calibrations are based on SDSS with small systematic errors which can be neglected in the following (Schlafly et al. 2012). (We checked that on a subsample of objects in common between SDSS and Pan-STARRS1 and found systematic errors in g, r, i, z magnitudes smaller than 0.1 mag.) V magnitudes in the Johnson-Cousins system are available from several sources, sometimes requiring some transformation, like NOMAD, UCAC4, Tycho-2, etc. with probably some unavoidable systematic errors when dealing with inhomo-

geneous sources. For those stars without V magnitude in the above catalogs, we can estimate them either from g, r, i in SDSS or Pan-STARRS1 using Lupton's formula, or from photographic B_J and R_F in the USNO-B1 catalog using Equations (5), (6) and Equation (7) recommended by Lépine & Shara (2005):

$$\begin{aligned} V &= B_J - 0.46(B_J - R_F), && (5)\\ V &= B - 0.23(B_J - J) - 0.10 \\ &\quad \text{for } B_J - J < 4; \\ V &= B - 0.05(B_J - J) - 0.72 \\ &\quad \text{for } B_J - J > 4, && (6)\\ V &= R_F + 0.6(R_F - J) - 0.10 \\ &\quad \text{for } R_F - J < 2; \\ V &= R_F + 1.10 \\ &\quad \text{for } R_F - J > 2, && (7) \end{aligned}$$

where the J magnitude is from 2MASS. The above three estimations of V are claimed by Lépine & Shara (2005) to be accurate to about $\pm$0.5 mag (yielding an error not larger than 25 $\%$ when used for distance estimates).

Extinction is an unavoidable issue when estimating distances. Schlegel et al. (1998) published an extinction map and the coefficient A_v was revised by Schlafly & Finkbeiner (2011). For objects with SDSS photometry, we attempted to obtain their extinction values in five bands of u, g, r, i, z directly, on the basis of the Schlegel et al. (1998) dust map. However, the Schlegel et al. (1998) dust map gives the extinction of the entire line of sight, leading to a significant overestimate for our nearby subdwarfs. As a matter of fact, we conclude that all the nearby sdMs have negligible extinction except those whose line-of-sight is along the direction of the Galactic anticenter. For those sources, we adopted the 3D extinction map by Chen et al. (2014). There is a translation of extinction coefficients in different bands as: $C_\lambda \equiv A_\lambda/A_r$ = 1.400, 0.759, 0.317, 0.200 and 0.132 for g, i, J, H, K bands, respectively (Yuan et al. 2013). The relation between A_r and A_z was found to be $A_z = 0.538A_r$. Table 3 lists the observed magnitudes and the adopted 3D extinction in the r band for our objects.

4.2 Photometric Distances

It is widely accepted that SdMs belong to the Milky Way thick disk population while the more metal-poor esdMs and usdMs belong to the halo (Lépine et al. 2007). To test this assertion using 3D Galactic motions or to search whether some sdMs could belong to the Galactic thin disk, we need to first estimate the distance of the objects in our sample.

In order to derive distances, we need to estimate absolute magnitudes. We build on previous work by Lépine & Shara (2005) and Bochanski et al. (2013). For high proper motion objects, the first authors derived an absolute magnitude-color relationship for the V band (Vega system), linking the magnitude M_V to the color $V - J'$.

They propose the following set of relations: Lépine & Shara (2005)

$$\begin{aligned} M_V &= 0.08 + 3.89(V-J) \ \text{ for } 0.7 < V - J < 1.5, \\ M_V &= 2.78 + 2.09(V-J) \ \text{ for } 1.5 < V - J < 3.0, \\ M_V &= 1.49 + 2.52(V-J) \ \text{ for } 3.0 < V - J < 4.0, \\ M_V &= 2.17 + 2.35(V-J) \ \text{ for } 4.0 < V - J < 5.0, \\ M_V &= 4.47 + 1.89(V-J) \ \text{ for } 5.0 < V - J < 9.0. \end{aligned} \quad (8)$$

The dispersion is about 0.35 to 0.7 mag depending on the range in $V - J$.

Alternately, we can use the method developed by Bochanski et al. (2013), based on the study of statistical parallaxes, to derive absolute magnitudes in r, i and z bands of SDSS or Pan-STARRS1, (AB system), with the following set of formulas

$$\delta_{(g-r)} = (g-r)_{\rm subdwarf} - (g-r)_{\rm dM}, \quad (9)$$

where $(g-r)_{\rm dM} = \sum_{i=0}^{6} C_n \times (r-z)^n$, and

$$\begin{aligned} M_{r,i,z} &= a_0 + a_1 \times (r-z) + a_2 \times (r-z)^2 + a_3 \\ &\quad \times \delta_{g-r} + a_4 \times (r-z) \times \delta_{(g-r)}. \end{aligned} \quad (10)$$

$\delta_{(g-r)} = (g-r)_{\rm subdwarf} - (g-r)_{\rm dM}$ is the color difference between a subdwarf and its solar metallicity counterpart as a function of the $r - z$ color. The coefficients a_i are given by Bochanski et al. (2013) for $0.8 < r - z < 3.6$.

Getting the absolute magnitude in four bands: V, r, i and z, we calculated four independent estimates of the distance from the standard relation: $D = 10^{0.2(m_{0x}-M_x)+1}$ (pc), where $m_{0x} = m_x - A_x$ is the de-reddened apparent magnitude of the star in the x band. Then we considered the average of the four values to be the true distance, and the standard deviation to be the error. Using the distance (D), the Galactic coordinates (l, b) and the consensus that the Sun is 15 pc above the Galactic plane and 8.5 kpc away from the Galactic center, we can derive the rectangular coordinates of the objects (X, Y, Z), where the value $Z + 15$ is the vertical distance from the object to the Galactic plane ($z_{\rm gal}$), and the norm of the vector ($X - 8500$, Y, $Z + 15$) is the distance to the Galactic center. The left panel of Figure 4 shows that, with its present sensitivity level, the LAMOST regular survey captures subdwarfs within 500 pc of the Sun, with 85$\%$ of the sample within 300 pc. This is quite close compared to the 1.5 kpc achieved by SDSS (Savcheva et al. 2014). Most subdwarfs in our sample are located within $\mid Z_{\rm gal} \mid \leq$350 pc. The right panel of Figure 4 does not show any obvious trend in metallicity index ζ with $Z_{\rm gal}$, a result to be expected because of the insufficient range of depth towards the halo inherent to our sample (see e.g. fig. 14 in Savcheva et al. 2014).

4.3 3D Galactic Motions

Based on the distance and proper motion (pm), the transverse velocity ($v_{\rm T}$) is computed by $v_{\rm T}$ = 4.74 $\times D$ (kpc) $\times\, pm$ (mas yr^{-1}). The distribution of $v_{\rm T}$ is shown in the

Table 5 Distances and Velocities

LAMOST ID	D (pc)	$Z_{\rm gal}$ (pc)	rpm (max yr^{-1})	dpm (max yr^{-1})	RV_P (km s^{-1})	RV_G (km s^{-1})	V_t (km s^{-1})	U (km s^{-1})	V (km s^{-1})	W (km s^{-1})	V_{tot} (km s^{-1})
J000530.87+031735.8	381	−307	6	8	−21	−88	18	0	189	85	207
J003010.59+400741.0	128	−34	140	−250	−53	−64	174	2	91	−117	148
J003023.63+050904.1	182	−138	−38	−204	−314	−260	179	173	−6	133	218
J003956.41+370159.1	91	−25	580	23	−16	−32	250	−194	78	17	210
J004143.13+312729.9	270	−126	212	14	−137	−150	272	−164	−16	88	187
J004613.83+335010.3	124	−45	890	−36	25	−14	524	−423	−69	−17	429
J005242.36+315545.1	203	−89	46	192	−145	−163	190	−5	169	247	300
J012100.34−012517.0	209	−172	−12	−388	−22	−40	385	220	−65	−127	262
J012534.63−041817.6	273	−234	46	−64	111	77	102	−24	150	−90	176
J012615.42+352030.6	241	−94	303	−53	−61	−83	351	−208	−58	36	219
J014614.53+010035.0	288	−232	−18	−78	19	29	109	63	174	−75	200
J022353.40+045251.3	285	−206	248	−90	202	225	356	−300	−31	−116	324
J023243.54+073557.0	336	−233	288	−98	132	135	485	−316	−155	−7	352
J023252.09+505139.4	-	-	−4	-	74	82	-	-	-	-	-
J023608.53+095440.9	234	−151	−16	−58	−91	−82	67	97	177	18	203
J024208.23+065529.0	204	−133	24	4	−37	−36	24	15	211	43	216
J030114.52+244228.6	159	−63	228	−64	100	89	178	−155	114	8	193
J031703.00+240118.8	240	−97	26	−160	−91	−117	184	118	51	−53	139
J032255.61+244336.5	185	−68	7	34	−2	−36	30	30	236	46	243
J032348.69+243229.4	199	−74	172	−56	124	89	171	−143	111	17	182
J034751.81+254730.6	108	−26	316	−293	−97	−111	221	53	−9	44	69
J035113.75+281105.1	207	−55	158	−142	144	189	208	−220	77	−59	241
J040301.53+153227.2	143	−50	180	−214	−278	−252	190	222	26	113	250
J041112.01+011826.0	-	-	158	−16	186	220	-	-	-	-	-
J041726.96+281947.9	82	−7	885	−336	7	103	368	−198	−67	130	246
J044738.31+273601.0	82	−1	122	−138	−24	9	72	−10	160	6	161
J050512.20+304322.8	259	−13	0	−8	180	171	10	−162	241	−20	291
J053434.17+221250.6	195	−4	44	−14	191	247	43	−238	178	8	298
J055612.53+243730.8	281	14	−292	64	166	138	398	−153	487	−289	586
J055710.69+343159.8	91	23	174	−298	−140	−163	149	160	71	−8	175
J061642.18+364838.6	73	27	−12	−34	38	61	12	−55	226	6	232
J062334.67+265644.1	337	52	12	20	79	178	37	−168	232	56	292
J062413.45+335651.4	393	81	208	−210	−151	−153	551	183	−294	151	378
J062500.70+305648.7	193	43	−60	−242	132	165	228	−171	49	−118	213
J063137.07+331035.6	286	68	54	−172	−66	−173	244	175	−9	−61	185
J063216.36+263137.5	308	57	34	−68	60	66	111	−44	112	14	121
J063257.83+323450.5	257	63	16	58	−44	−44	73	58	287	44	296
J063347.51+235036.2	81	25	6	4	17	57	3	−48	221	15	227
J065045.65+521346.8	21	23	46	−336	90	120	34	−112	230	43	259
J070025.94+265335.1	332	94	84	−72	55	132	174	−76	57	110	145
J071033.86+271818.2	262	87	11	12	51	−194	20	194	272	−31	335
J071424.09+273918.4	64	34	216	−438	−39	−33	148	67	91	5	113
J071753.80+354038.8	-	-	10	−341	133	151	-	-	-	-	-
J071758.85+354257.0	-	-	8	2	74	68	-	-	-	-	-
J072320.04+253610.9	144	59	−80	−208	391	428	152	−397	25	38	399
J072516.99+290323.3	65	37	119	8	95	104	37	−76	205	73	231
J073835.27+343953.5	207	100	116	−134	−140	−157	174	192	86	4	210
J074444.97+272648.2	310	137	−22	6	104	81	34	−80	230	11	244
J074655.54+281323.6	327	147	0	8	25	7	12	0	241	12	241
J074656.72+215025.9	93	49	50	−226	154	161	102	−108	85	49	146
J075423.94+290739.1	328	157	16	−76	206	209	121	−158	73	84	193
J075852.18+215135.0	298	137	−50	−224	75	81	324	−41	−74	−126	151
J075920.76+525928.1	124	80	−28	12	21	58	18	−47	253	22	258
J080633.27+321145.4	144	85	−223	−510	90	93	380	−140	−93	−159	232
J083012.38+332105.1	144	96	130	−310	−192	−103	229	151	25	−18	154
J084127.90−011403.2	59	39	−40	−44	85	116	17	−66	144	37	162
J084542.20+252123.5	243	156	−48	−28	355	337	64	−280	110	150	336
J084601.17+272302.0	156	107	−104	−432	71	55	329	−37	−86	−89	130
J091406.72+305034.3	108	88	−76	−50	−2	18	47	−29	201	−14	204

Table 5 — *Continued.*

LAMOST ID	D (pc)	$Z_{\rm gal}$ (pc)	rpm (max yr^{-1})	dpm (max yr^{-1})	RV_P (km s^{-1})	RV_G (km s^{-1})	V_t (km s^{-1})	U (km s^{-1})	V (km s^{-1})	W (km s^{-1})	V_{tot} (km s^{-1})
J092725.42+171101.0	267	194	58	−232	27	26	303	137	−44	−6	144
J093756.59+283917.0	241	193	−8	14	62	109	18	−73	221	81	246
J093941.97+275140.9	210	170	−50	−200	22	41	205	−13	24	−22	35
J095451.13+085152.7	186	145	8	−38	−28	−38	34	44	223	−29	229
J095805.56+333801.5	324	271	92	−134	−7	−46	250	183	53	51	197
J101247.46+274729.5	168	153	−14	−116	−48	−51	93	50	151	−51	167
J102351.13+320401.8	112	110	−220	−138	−6	−36	138	−52	140	−89	174
J102516.09+461745.8	163	149	−28	18	33	39	26	−34	243	23	247
J103528.96+423846.0	84	87	−26	−44	1	20	20	−9	212	20	213
J104049.04+290539.3	113	114	−34	−266	4	44	144	15	82	30	89
J104352.42+303649.3	270	253	166	−122	−55	−68	264	263	146	44	304
J104521.52+482823.3	-	-	−6	20	101	51	-	-	-	-	-
J105220.46+274313.1	287	272	40	−156	106	93	219	87	28	103	138
J105240.29+283353.8	305	289	−2	12	65	56	18	−24	236	54	243
J105736.90+473807.5	167	159	10	−88	−88	−39	70	46	161	−7	167
J105753.97+272644.0	410	386	−22	16	23	1	53	−41	246	−11	250
J110717.83+273252.0	125	130	−6	−4	7	−13	4	9	229	−8	229
J112129.19+073443.2	259	242	−66	−262	77	113	332	69	−112	−34	137
J112811.03+535521.6	259	237	−174	−178	1	57	306	−153	−27	75	173
J113108.72+540535.4	399	358	−86	−20	49	44	167	−145	148	9	207
J115646.82+593904.9	230	206	−30	−84	−113	−211	97	88	59	−130	167
J115914.12+580528.5	149	141	−72	−162	−175	−160	125	58	55	−84	116
J120229.03+264514.8	74	88	8	14	1	−4	6	8	236	2	236
J121434.23+584523.4	161	151	−96	−122	−70	−79	118	4	91	−24	94
J121546.28+324433.1	321	332	−208	−60	10	−48	329	−217	−2	−78	230
J121956.41+273337.9	245	258	−94	−18	6	4	111	−78	159	−4	177
J123045.52+410943.8	76	89	2	−32	11	−18	12	17	218	−10	219
J124754.95+114026.0	134	144	0	−83.8	31	20	53	37	182	10	186
J125203.78+540656.1	174	170	172	−392	32	−230	353	340	−22	−54	345
J125207.81+003708.6	189	184	−14	20	3	−24	22	−18	246	−8	247
J125648.36+394429.1	68	81	−14	12	−6	0	6	1	231	4	231
J131006.33+201951.7	81	95	−62	6	50	77	24	−4	214	83	230
J131754.25+191846.2	129	142	−32	−402	96	69	247	143	16	41	149
J132823.09+090226.8	95	104	54	6	−5	15	24	29	244	16	247
J133222.33+185719.8	131	143	−86	−256	−88	−104	168	36	73	−111	138
J140505.50+162647.2	296	293	42	−146	30	14	213	178	110	−39	213
J141935.25+504216.3	102	104	−104	−36	−75	−57	53	−13	160	−22	162
J142332.60+231801.0	213	214	−58	22	103	74	63	−24	221	96	242
J142714.04+335957.7	230	229	−288	−222	−87	−50	396	−38	−158	91	186
J145636.05+312454.7	353	328	−14	−130	−146	−133	219	117	24	−101	156
J145811.86+311508.5	188	181	−285	−44	−22	−42	257	−125	21	87	153
J151637.89+340322.6	195	181	−74	−46	−9	4	81	6	160	45	167
J154919.39+001316.1	54	49	−74	10	−82	−81	19	−64	211	−34	223
J170252.10+330952.2	-	-	−16	84	−135	−152	-	-	-	-	-
J172012.34+242931.7	75	53	−252	−269	−98	−75	131	31	81	15	88
J220747.72+001606.0	248	−151	−56	−122	−250	−240	158	43	−22	138	146
J225612.76+061236.3	158	−100	58	−76	−64	−81	72	−12	124	15	126
J230312.72+044430.7	289	−202	148	34	−108	−143	208	−208	107	55	240
J235409.68+281720.2	63	−19	−2	−334	−188	−230	100	108	5	49	119

Notes: '-' are default values for those objects whose distance cannot be estimated accurately. RV_P means RVs from the pipeline and RV_G means RVs from Gaussian fitting.

Table 6 Supplemental Information on Active sdMs

LAMOST ID	EW(Hα)	S/N$_r$	S/N$_i$
J041112.01+011826.0	0.93	16.0	30.4
J061642.18+364838.6	1.16	85.8	148.3
J065045.65+521346.8	1.54	23.1	58.4
J084127.90-011403.2	0.77	19.7	27.9
J104521.52+482823.3	4.42	4.0	6.7
J120229.03+264514.8	1.11	18.8	32.1
J123045.52+410943.8	2.72	3.5	6.1

left panel of Figure 6. Most stars have transverse velocities smaller than 400 km s^{-1}. The high velocity tail of the histogram is due to some unrealistic distance estimates. Heliocentric radial velocity (RV) is another basic parameter of an object, for it is a projection of the 3D velocity along the line of sight and can be measured from the spectrum. The RVs of the sdMs from LAMOST DR2 have been measured by the LAMOST 1D pipeline. Because the pipeline estimates RVs based on cross-correlating the target spectrum with a rest-frame template spectrum (Tonry & Davis 1979), we also provide another version of RVs for all the candidates in our sample by fitting single Gaussian profiles to a set of absorption lines, see Table 4. A histogram of RVs is seen in the right panel of Figure 6. Nearly all our sdMs are found within ± 200 km s^{-1}. The two algorithms show good consistency (Fig. 5). However, the RVs from the pipeline might be inaccurate since the templates in the LAMOST pipeline are all based on spectra from stars with solar abundance (just like SDSS) so there is potential mismatch (Savcheva et al. 2014). So, here we adopted the RVs derived from Gaussian line fitting, since they are more accurate for single stars.

3D Galactic motions (also called 3D space velocities) are the projections of the total velocity vector of the star on the three directions (U, V, W) of the classic Galactic coordinate system. The velocities are determined by the object's distance, RV, pm and coordinates, and must be corrected for the solar motion $(U, V, W)_\odot$ = (7.01, 10.13, 4.95) km s^{-1} (Huang et al. 2015). The small size of our sample does not enable us to make a detailed analysis. Here, we just produce the histograms of the 3D motion for all the sdMs (Fig. 7). The U velocity distribution (component radially directed towards the Galactic center) is symmetric, peaks at zero and is basically restricted within ±300 km s^{-1}. The W velocity distribution (component towards the North Galactic Pole) is similar to the U one, with a dispersion of 80 km s^{-1}. The V velocity distribution differs from the other two; it represents the motion around the Galactic center and it is an asymmetric distribution. The youngest populations of the thin disk are known to have a small V component centered around –20 km s^{-1} with a small dispersion. Here, the bulk of the sample, clearly more dispersed, is constrained between –50 and 250 km s^{-1} in V.

All the distance and velocity information is listed in Table 5.

5 PECULIAR OBJECTS

5.1 Active Objects

Among our 108 sdMs, a handful exhibit a significant Hα emission line, indicating chromospheric activity (Hawley et al. 1996).

We measured the equivalent width (EW) of the Hα line according to West et al.: line center at 6564.66 Å, line width 8 Å, blue continuum 6555–6560 Å, and red continuum 6570–6575 Å. Then we selected the stars as active ones when they met the following four conditions:

(1) EW (Hα) > 0.75 Å;
(2) Uncertainty of EW (Hα) $<$ EW (Hα);
(3) S/N at H$\alpha > 3$;
(4) The peak of the Hα line is three times higher than the nearby 'continuum' fluctuation.

Seven active sdMs were found, including one esdM. We list their properties (Table 6) and present their spectra in the left panel of Fig. 8. A peculiar active sdM in a binary system is discussed below. Another unusual star is LAMOST J123045.52+410943.8 which shows several hydrogen Balmer lines in emission and carbon features in the red part, with a marked CN absorption band near 7800–8000 Å. Spectrum 1984-53433-365 in SDSS fully confirms this and shows the Balmer series in emission till H10, also with a bright violet CaII doublet in emission.

5.2 White Dwarf – M Subdwarf Binary: LAMOST J104521.52+482823.3

LAMOST J104521.52+482823.3 shows strong Balmer lines in absorption, which are not supposed to exist in M type spectra. It seems that a hotter star and an M type star appear in the same spectrum (right panel of Fig. 8). The usual interpretation of this kind of spectrum is that of a binary system with a DA (hydrogen-rich) white dwarf and an M dwarf. This object has been previously listed by Ren et al. (2014) as a white dwarf - main sequence binary. However, the secondary star appears clearly not to be an ordinary main sequence M dwarf, but rather an M subdwarf. It could provide useful clues in understanding star formation processes and dynamical evolution in the Galaxy.

According to Ren et al. (2014), the primary star is a white dwarf with a $T_{\rm eff} \approx 19\,900$ K, log g ≈ 8.77, mass $\approx$1.09 $M_\odot$ and a distance to us of about 218 pc, with the secondary being type M3. New fitting of the DA models enabled us to revise the $T_{\rm eff}$ of the white dwarf to 10 500 K, the log g to 8.51 and the subclass of the secondary star to sdM3. The spectrum (right panel of Fig. 8) shows a strong Hα emission line, but it cannot be confirmed if it is caused by the chromospheric activity of the sdM. An Hβ emission line is also visible, as well as HeI 5876 Å in emission. The ultraviolet spectrum appears very flat (GALEX fuv, nuv and SDSS u magnitudes (all in the AB system) are respectively 18.39, 18.61 and 18.77) but a search in X-ray archival catalogs did not yield results. We also suspect an accretion disk around the white dwarf to be the cause of the emission line activity, but further and deeper observations are needed to confirm or refute this hypothesis.

6 SUMMARY AND CONCLUSIONS

We identify a sample of 108 nearby M subdwarf stars from the LAMOST DR2, including 64 ordinary sdMs, 33 esdMs and 11 usdMs. Due to the limiting magnitude of the

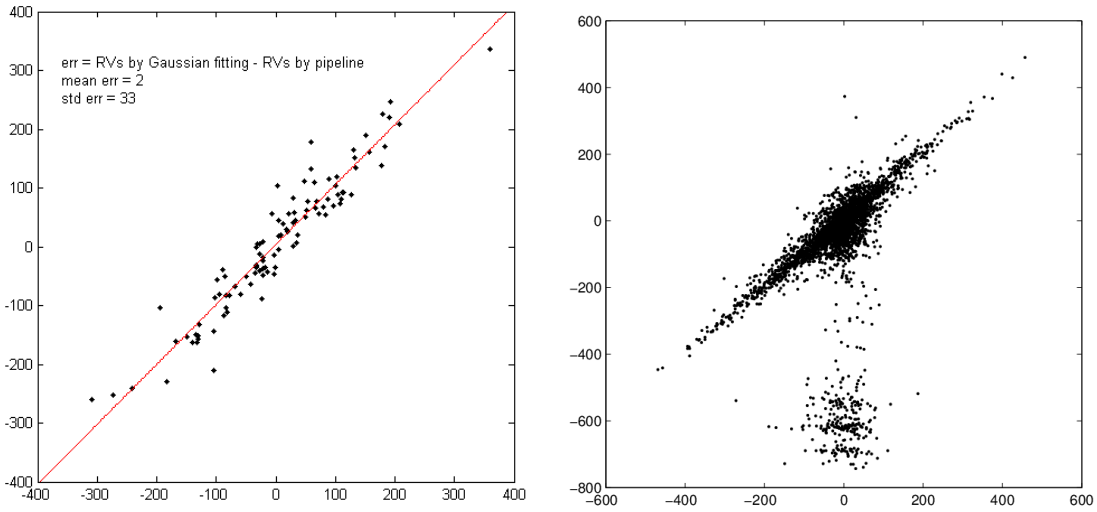

Fig. 5 Comparison of radial velocities measured by two methods. *Left panel*: LAMOST sample: X-axis: RVs from the LAMOST pipeline with the cross-correlation method by Tonry & Davis (1979), Y-axis: RVs from Gaussian spectral line fitting. *Right panel*: SDSS sample (Savcheva et al. 2014): X-axis: RVs from the SDSS pipeline (cross correlation), Y-axis: RVs revisited by Savcheva et al. (2014). The main cloud is fitted by the linear relation $Y = 0.93X - 8.8$.

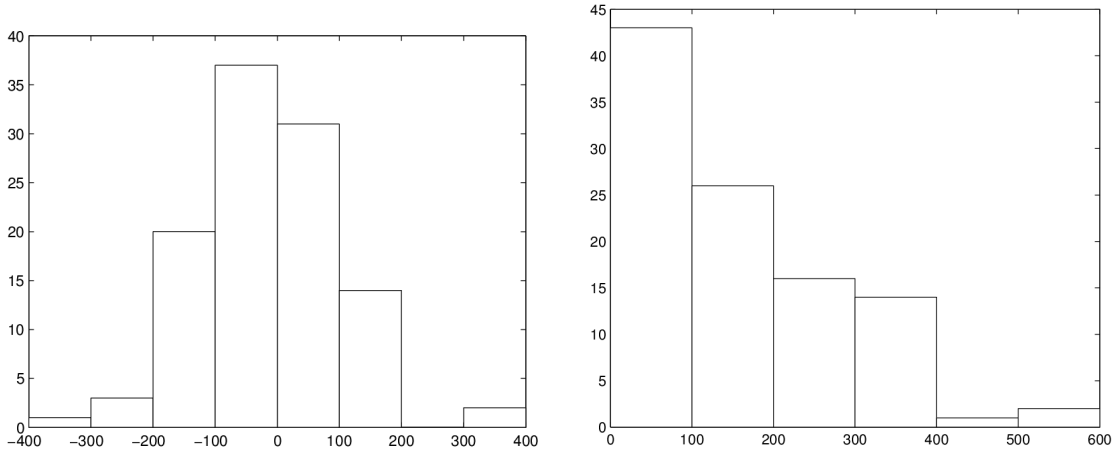

Fig. 6 *Left panel*: Histogram of transverse velocities of all sdMs in our sample. *Right panel*: Distribution of their radial velocities. It peaks at zero and has a dispersion of about 115 km s^{-1}.

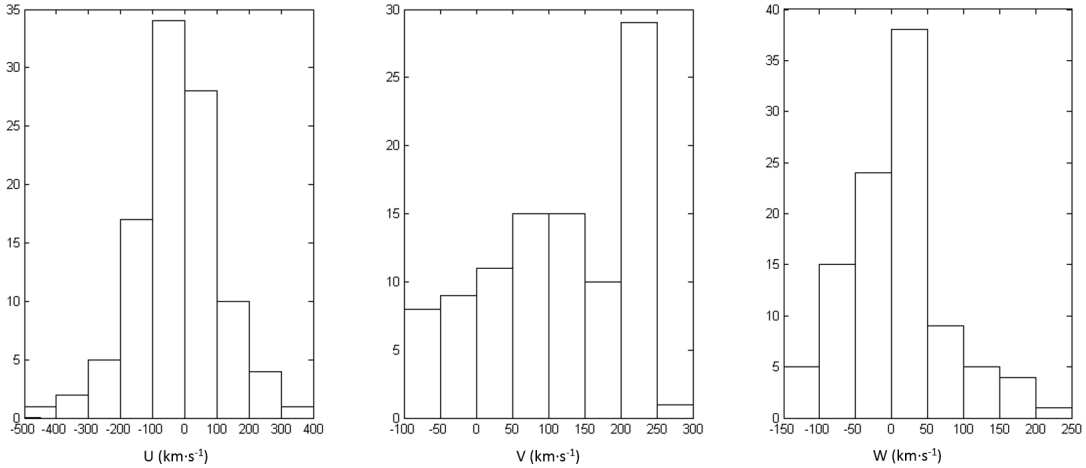

Fig. 7 Histograms of the 3D velocities U, V and W, from left to right respectively.

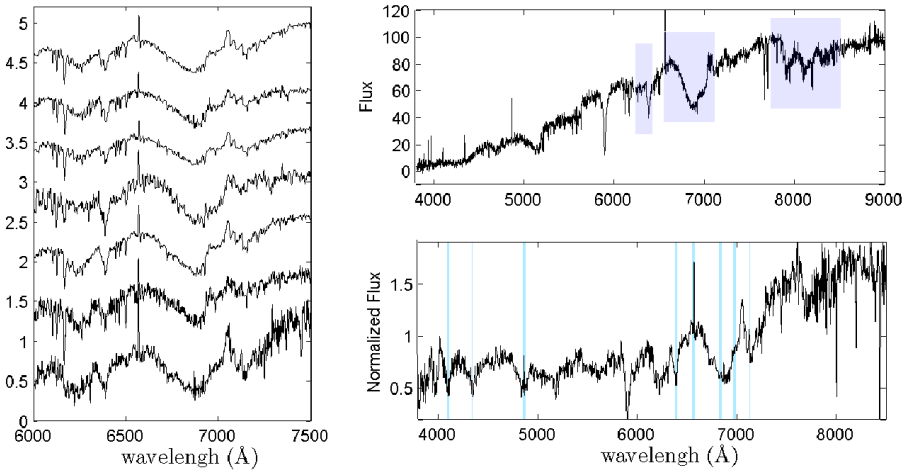

Fig. 8 *Left panel*: LAMOST spectra of the seven active sdMs with strong Hα emission. *Right top panel*: SDSS spectrum 1984-53433-365 of an active usdM (the fourth one from the top in the left panel), with significant carbon features. *Right bottom panel*: the binary system LAMOST J104521.52+482823.3, a white dwarf and an sdM. Note that besides a strong Hα emission line, there is also significant Hβ and HeI emission lines (magenta). All the features are marked in the figure.

LAMOST survey, only quite bright, early M type sdMs can be picked out (not cooler than M3, or $T_{\rm eff} < 3300$ K). In addition to the SPT and the Lépine et al. metallicity index ζ, we also present the effective temperature and the [Fe/H] of the sdMs derived from a comparison with PHOENIX model spectra. Both correlations of the index ζ vs. [Fe/H] and the SPT vs. $T_{\rm eff}$ exhibit reasonable consistency. The average metallicities [Fe/H] of sdMs, esdMs and usdMs are –0.5, –1 and –1.5 respectively, confirming the metallicity hierarchy in our sample, in agreement with previous works. To estimate the distances, we use the magnitude in 11 bands: g, r, i, z, J, H, K, B, R, I and V. For objects located toward the Galactic anticenter, we adopted the 3D extinction from Chen et al. (2014). Other sources were supposed to suffer negligible extinction because of their small distance. Most of our sdMs are located within 500 pc of the Sun and 350 pc of the Galactic plane, closer than those selected by the SDSS survey whose limiting magnitude is fainter. Kinematical information is available from radial velocities and proper motions. We compute estimates of total velocities and 3D Galactic motions. We have positive detections of an Hα emission line in seven sdMs, including one esdM. LAMOST J104521.52+482823.3 is a DA white dwarf - sdM binary; there is still not enough evidence to understand the physical mechanism causing the emission lines. LAMOST J123045.52+410943.8, also active with several Balmer emission lines, exhibits carbon features in its red spectrum.

Acknowledgements This work is partly supported by the National Key Basic Research Program of China (Grant No. 2014CB845700) and the National Natural Science Foundation of China (Grant No. 11390371). The Guo Shou Jing Telescope (the Large Sky Area Multi-Object Fiber Spectroscopic Telescope, LAMOST) is a National Major Scientific Project built by the Chinese Academy of Sciences. Funding for the project has been provided by the National Development and Reform Commission. LAMOST is operated and managed by National Astronomical Observatories, Chinese Academy of Sciences.

References

Allard, F., & Hauschildt, P. H. 1995, ApJ, 445, 433
Bochanski, J. J., Savcheva, A., West, A. A., & Hawley, S. L. 2013, AJ, 145, 40
Chen, B.-Q., Liu, X.-W., Yuan, H.-B., et al. 2014, MNRAS, 443, 1192
Covey, K. R., Ivezić, Ž., Schlegel, D., et al. 2007, AJ, 134, 2398
Cui, X.-Q., Zhao, Y.-H., Chu, Y.-Q., et al. 2012, RAA (Research in Astronomy and Astrophysics), 12, 1197
Eggen, O. J., & Greenstein, J. L. 1965, ApJ, 142, 925
Giclas, H. L., Burnham, R., & Thomas, N. G. 1971, Lowell Proper Motion Survey Northern Hemisphere. The G Numbered Stars. 8991 Stars Fainter than Magnitude 8 with Motions $>$ $0.26''$/year (Flagstaff, Arizona: Lowell Observatory)
Gizis, J. E. 1997, AJ, 113, 806
Hawley, S. L., Gizis, J. E., & Reid, I. N. 1996, AJ, 112, 2799
Huang, Y., Liu, X.-W., Yuan, H.-B., et al. 2015, MNRAS, 449, 162
Kaler, J. B. 1989, Stars and Their Spectra. An Introduction to Spectral Sequence (Cambridge: Cambridge University Press)
Laughlin, G., Bodenheimer, P., & Adams, F. C. 1997, ApJ, 482, 420
Lépine, S., Hilton, E. J., Mann, A. W., et al. 2013, AJ, 145, 102
Lépine, S., Rich, R. M., & Shara, M. M. 2003, AJ, 125, 1598
Lépine, S., Rich, R. M., & Shara, M. M. 2007, ApJ, 669, 1235
Lépine, S., & Shara, M. M. 2005, AJ, 129, 1483

Luo, A.-L., Zhao, Y.-H., Zhao, G., et al. 2015, RAA (Research in Astronomy and Astrophysics), 15, 1095
Luyten, W. J. 1976, LHS (Luyten half-second) Catalogue., by Luyten, W. J. (Univ. Minnesota, Minneapolis, Minnesota)
Luyten, W. J. 1979, New Luyten Catalogue of Stars with Proper Motions Larger than Two Tenths of an Arcsecond; and First Supplement; NLTT (Minneapolis 1979)
Monet, D. G., Levine, S. E., Canzian, B., et al. 2003, AJ, 125, 984
Mould, J. R. 1976, ApJ, 207, 535
Reid, I. N., Hawley, S. L., & Gizis, J. E. 1995, AJ, 110, 1838
Ren, J. J., Rebassa-Mansergas, A., Luo, A. L., et al. 2014, A&A, 570, A107
Salim, S., & Gould, A. 2003, ApJ, 582, 1011
Savcheva, A. S., West, A. A., & Bochanski, J. J. 2014, ApJ, 794, 145
Schlafly, E. F., & Finkbeiner, D. P. 2011, ApJ, 737, 103
Schlafly, E. F., Finkbeiner, D. P., Jurić, M., et al. 2012, ApJ, 756, 158
Schlegel, D. J., Finkbeiner, D. P., & Davis, M. 1998, ApJ, 500, 525
Skrutskie, M. F., Cutri, R. M., Stiening, R., et al. 2006, AJ, 131, 1163
Tonry, J., & Davis, M. 1979, AJ, 84, 1511
West, A. A., Morgan, D. P., Bochanski, J. J., et al. 2011, AJ, 141, 97
Woolf, V. M., Lépine, S., & Wallerstein, G. 2009, PASP, 121, 117
York, D. G., Adelman, J., Anderson, Jr., J. E., et al. 2000, AJ, 120, 1579
Yuan, H. B., Liu, X. W., & Xiang, M. S. 2013, MNRAS, 430, 2188